HHS Public Access

Author manuscript

Nat Biomed Eng. Author manuscript; available in PMC 2017 October 18.

Published in final edited form as:

Nat Biomed Eng. 2017 ; 1: . doi:10.1038/s41551-017-0040.

Light scattering spectroscopy identifies the malignant potential of pancreatic cysts during endoscopy

Lei Zhang[1,†], **Douglas K. Pleskow**[2,†], **Vladimir Turzhitsky**[1], **Eric U. Yee**[3], **Tyler M. Berzin**[2], **Mandeep Sawhney**[2], **Shweta Shinagare**[3], **Edward Vitkin**[1], **Yuri Zakharov**[1], **Umar Khan**[1], **Fen Wang**[2], **Jeffrey D. Goldsmith**[3], **Saveli Goldberg**[4], **Ram Chuttani**[2], **Irving Itzkan**[1], **Le Qiu**[1,*], and **Lev T. Perelman**[1,2,5,*]

[1]Center for Advanced Biomedical Imaging and Photonics, Department of Obstetrics, Gynecology and Reproductive Biology, Harvard University, Boston, Massachusetts 02215 USA

[2]Division of Gastroenterology, Department of Medicine, Harvard University, Boston, Massachusetts 02215 USA

[3]Department of Pathology, Beth Israel Deaconess Medical Center, Harvard University, Boston, Massachusetts 02215 USA

[4]Division of Biostatistics and Biomathematics, Massachusetts General Hospital, Harvard University, Boston, Massachusetts 02215 USA

[5]Biological and Biomedical Sciences Program, Harvard University, Boston, Massachusetts 02215 USA

Abstract

Pancreatic cancers are usually detected at an advanced stage and have poor prognosis. About one fifth of these arise from pancreatic cystic lesions. Yet not all lesions are precancerous, and imaging tools lack adequate accuracy for distinguishing precancerous from benign cysts. Therefore, decisions on surgical resection usually rely on endoscopic ultrasound-guided fine needle aspiration (EUS-FNA). Unfortunately, cyst fluid often contains few cells, and fluid chemical analysis lacks accuracy, resulting in dire consequences, including unnecessary pancreatic surgery for benign cysts and the development of cancer. Here, we report an optical spectroscopic technique, based on a spatial gating fibre-optic probe, that predicts the malignant potential of pancreatic cystic lesions

*Correspondence and requests for materials should be addressed to L.Q. (lqiu@caregroup.harvard.edu) and L.T.P. (lperelman@fas.harvard.edu).

†These authors contributed equally to this work.

Author contributions

L.Q., D.K.P and L.T.P. conceived the method and initiated the project; L.Q. and L.T.P. supervised the project; L.Q., L.Z., U.K. and Y.Z. constructed the system; D.K.P., R.C., M.S., and T.M.B. performed clinical procedures; L.Z., Y.Z., U.K., and L.Q. performed measurements; E.U.Y., S.S., and J.D.G evaluated the histology specimens; E.V. performed the data analysis; L.Z., E.Y., V.T., J.D.G., F.W., L.Q. and L.T.P. evaluated the method; S.G. performed statistical analysis; V.T., I.I., T.M.B., L.Z., and L.Q. contributed to the writing of the manuscript; L.T.P. wrote the manuscript.

Supplementary information is available for this paper.

Competing financial interests

The authors declare no competing financial interests.

during routine diagnostic EUS-FNA procedures. In a double-blind prospective study in 25 patients, with 14 cysts measured *in vivo* and 13 postoperatively, the technique achieved an overall accuracy of 95%, with a 95%confidence interval of 78–99%, in cysts with definitive diagnosis.

Graphical Abstract

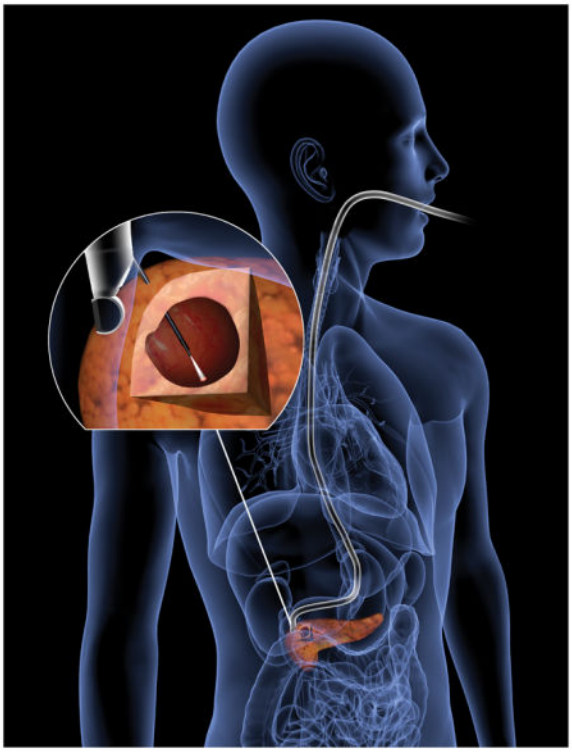

Pancreatic cancer has the lowest survival rate among all major cancers, typically six months from diagnosis[1]. This is due to an inability to detect it early, while still treatable, largely because of the inaccessible location of the pancreas deep in the abdomen. Also, the disease often metastasizes while it is still asymptomatic[2]. About one fifth of pancreatic cancers arise from cystic lesions that can potentially be identified in early, treatable stages with non-invasive imaging techniques such as computed tomography (CT) and magnetic resonance imaging (MRI). Cystic lesions are relatively common, occurring in at least 2% of adults[3], with some studies describing the incidental finding of pancreatic cysts in more than 10% of abdominal MRIs obtained for non-pancreatic indications[4]. It should therefore come as no surprise that cystic lesions account for one third of all pancreatic surgeries[5]. However, while CT and MRI could be used to screen for cystic lesions, they have limited accuracy with regard to identifying the type of pancreatic cyst. Currently, there is no sufficiently accurate diagnostic technique that can reliably distinguish cancerous and pre-cancerous cysts from benign cysts. The resulting uncertainty in diagnosis of pancreatic cystic lesions can lead to a delay in surgical resection of precancerous lesions, as well as unnecessary surveillance and even surgery for benign cysts. Considering the high mortality and morbidity of pancreatic surgeries and the even higher mortality from untreated pancreatic cancers, there is an

obvious need for the development of new diagnostic methods to accurately identify pancreatic cysts that need surgical intervention.

The best currently available diagnostic method for identifying malignancy in pancreatic cyst lesions is based on the minimally invasive EUS-FNA procedure, which is performed in at least 90% of cases when the decision to undergo surgery is required. This procedure has an overall sensitivity of less than 50% for detecting malignancy with the majority of results being non-diagnostic[6,7]. During the EUS-FNA procedure the cyst fluid is collected and then analyzed both for tissue (cytopathology) evaluation, and also for the presence of certain molecular markers or glycoproteins, such as carcinoembryonic antigen (CEA).

There are two primary types of precancerous pancreatic cystic lesions, intraductal papillary mucinous neoplasms (IPMN), and mucinous cystic neoplasms (MCN)[8,9], that could be treated surgically, achieving a high cure rate. However, the majority of cystic pancreatic lesions have no malignant potential and do not require surgery. Certain types of precancerous cysts can be safely monitored over years, and may not require surgical resection. Higher risk precancerous cysts should be removed surgically, prior to cancer development. Pancreatic surgery is complex and is associated with significant morbidity and mortality. For instance, the Whipple procedure, also known as pancreatoduodenectomy, involves removing the head of the pancreas, two thirds of the duodenum, and one third of the stomach and has a mortality rate of more than 11% when averaged over all the US hospitals[10]. Therefore, the decision to consider surgery for a pancreatic cyst requires the treating physician to weigh data from potentially inaccurate EUS-FNA results with several even less conclusive imaging tests and with the patient's ability to tolerate the surgery. As a result, of the pancreatoduodenectomies which are performed on cystic lesions, only about 42% are later confirmed as featuring precursor lesions with malignant potential[11]. On the other hand, precancerous and small resectable cancerous cysts, when left untreated, have the risk of progressing to incurable cancer.

There is a critical need for the development of a diagnostic method that improves the accuracy of cyst evaluation and can be employed during the EUS-FNA procedure. The basic physical principle that elastic light scattering can distinguish pre-cancerous and early cancerous lesions was demonstrated earlier[12]. There are three main components of tissue light scattering spectra. The largest is a diffuse background signal from submucosal tissue, next is scattering by small organelles and lastly a relatively small backscattered component from epithelial cell nuclei. The submucosal background can be excluded by one of various gating techniques[12–18] and the smaller organelles have a very different scattering spectral dependence than that of the nuclei. Elastic light scattering can also be used to measure other cellular compartments, such as mitochondria[19], whose spectra[20] are sufficiently different from that of nuclei to be distinguished[21]. The combination of gating and difference in spectral behavior allows the epithelial nuclear scattering spectrum to be isolated in the processed light scattering spectroscopy (LSS) signal. A significant contribution from nuclear backscattering and clear correlation of dysplasia with nuclear size has been demonstrated in earlier studies[12–16,22–24]. Direct comparison of the nuclear size distribution extracted from the backscattering signal to that of histological examination of the corresponding H&E stained sections was also demonstrated[17,18].

Now we have developed a new instrument that uses this principle to solve the difficult problem of identifying pre-cancerous and early cancerous lesions in the pancreas. The instrument can probe the internal surface of pancreatic cysts, obtaining multiple noninvasive optical “biopsies” from each cyst in a matter of seconds, performing significantly better than existing cytology and cyst fluid CEA markers. Our results indicate that this technology has significant potential to aid in identifying both precursor lesions and early stage pancreatic cancers.

Results

In order to develop an *in vivo* LSS system and diagnostic algorithm, we first performed a pilot *ex vivo* study to evaluate the ability of LSS to differentiate cystic neoplasms with varying grades of malignancy from benign cysts. We then designed a needle-based LSS instrument for *in vivo* use during EUS-FNA procedures and have recently collected spectra from the pancreatic cysts of 14 consecutive subjects who satisfied the study enrollment criteria. The diagnostic cut-offs were determined prospectively and the experimenters performing the data collection and analysis were blinded to the patient diagnosis, while the gastroenterologists making the patient diagnosis were blinded to the LSS results.

Studies in freshly resected pancreatic samples

Measurements on freshly resected pancreatoduodenectomy and distal pancreatectomy samples from 11 subjects including a total of 13 pancreatic cystic lesions were obtained. The LSS spectra from pancreatic resection samples were measured with the clinical LSS system and polarization gated probe, developed previously for Barrett’s esophagus (BE) studies[13]. The spectra were collected from multiple locations with the measured sites marked with India ink, and photographed to ensure proper co-registration with the subsequent histopathology examination. To differentiate various cystic neoplasm histopathologies we employed the diagnostic parameter Δ introduced in our BE studies[13], with the only difference in that the root mean square normalized spectrum, employed in the diagnostic algorithm, was now calculated using all cystic lesion measurements. In our BE studies, if this diagnostic parameter was greater than 0.1 (10% of the mean squared spectrum summed over all spectral points), the site was considered to be dysplastic. Following the same logic, our diagnostic criteria for cystic lesions classified $\Delta<0.1$ as benign, $0.1<\Delta<0.2$ as low-grade dysplasia (LGD), and $\Delta>0.2$ as high-grade dysplasia (HGD). The cut-offs $\Delta=0.1$ and $\Delta=0.2$ correspond to 25% and 50% enlarged nuclei according to our earlier work[13]. The use of the same diagnostic criteria as in the BE studies is rationalized by the fact that the two most common types of precancerous pancreatic cystic lesions, IPMN and MCN, are characterized by a similar type of lining as in the BE, columnar epithelium. The data analysis was performed in a double-blind manner, prior to postoperative histopathology results becoming available. The preoperative cytology results and CEA levels were not taken into account.

To check if LSS would improve the diagnosis of cystic neoplasms, we compared our findings with preoperative imaging results, cytology results and cyst fluid CEA levels as well as postoperative histopathology, which was considered the gold standard. These results are summarized in Table 1 and discussed below.

In all cases, LSS diagnosis of benign and dysplastic cysts agreed with histopathology. When dysplasia grades were taken into account, 2 benign cases, 4 LGD cases and 6 HGD cases were correctly identified while one HGD case was identified as LGD. Figure 1e shows a summary of the diagnostic parameter values as bars that are colored according to final histopathology diagnosis. *In vivo* CT and Magnetic Resonance Cholangiopancreatography (MRCP) images of cystic lesions 1 and 6 are shown in Figures 1a and b, circled in red. Photographs of the same cysts are shown in Figures 1c and d, respectively. For example, the first subject had a 1.3 cm × 2.3 cm cystic lesion within the pancreatic tail, which was detected via abdominal and pelvic CT angiography (Fig. 1a) and described as a possible side-branch IPMN. EUS-FNA cyst fluid resulted in a CEA of 686 ng/ml, significantly higher than the 192 ng/ml cut-off suggestive of a mucinous lesion[6,25]. Cytology reported scant acellular debris which could not be further categorized. Though the CEA level and cytology results were inconclusive for cancer, these results, along with the size of the cyst and clinical findings, were considered worrisome enough to warrant pancreatic surgery. LSS spectroscopy performed on the freshly resected cyst diagnosed all 7 locations within the cyst as LGD and later postoperative histopathology findings for all 7 locations were indeed IPMN with LGD. The other cyst measurements showed similar correlations with histopathology.

To summarize, this double-blind *ex vivo* study in cysts, representing 3 out of 4 primary types of pancreatic lesions (IPMN, serous cystadenoma, and pseudocyst, but not MCN), demonstrated 92% accuracy, with a 95% confidence interval (CI) of 67–99%, when dysplasia grades are taken into account and 100% accuracy (95% CI: 77–100%) when identifying dysplastic vs. benign cysts, suggesting that the proposed technique is accurate. By comparison, the accuracy of MRI/CT imaging, as determined from the patient cohort within our study, was only 54% for identifying dysplasia grade when compared with postoperative histopathology. Note that the percentage of premalignant cysts in our study is higher than that in the general population because our cohort was composed of pancreatic resection samples.

In vivo EUS-FNA clinical system

Detecting malignancies with LSS requires separating the backscattering signal coming from the epithelial cells from the multiple scattering signal coming from the underlying connective tissue. Accessing the cystic lesions required developing a new probe with a diameter that can fit into a standard 22 gauge (0.54 mm internal diameter) and 19 gauge (0.91 mm internal diameter) aspiration needles. Such a compact package polarization gated probe is technologically challenging. Instead we developed the “spatial gating probe” (Fig. 2 and Methods), which is significantly easier to build and allows measurement of the backscatter signal. This probe uses the fact that the backscatter signal coming from the epithelial cells decreases significantly faster than the multiple scattering signal. Use of this probe requires an invertible theory that accurately describes reflectance signals from fibers separated by distances smaller than the inverse of the reduced scattering coefficient. The classical diffusion approximation[26] will not work since it fails to take into account the contribution of photons which have undergone several low-angle scattering events plus a single large-angle scattering event. It is precisely these photons which are sensitive to the

structure of the epithelial layer. Fortunately, our recently published work[27] solves this long-standing problem in radiative transport[28,29], and provides a highly accurate analytic expression for the spatially dependent reflectance near the point of entry and provides a means to evaluate the backscatter signal from the signals measured by the spatial gating probe. This allows obtaining the same diagnostic parameter, Δ, from spatially gated data that we used with polarization gated data (see Methods).

Differentiating cystic lesions *in vivo*

We performed clinical *in vivo* measurements using spatial gating LSS during routine EUS-FNA procedures in 14 consecutively enrolled subjects with pancreatic cysts. Prior to the procedure the spatial gating probe was inserted in the 22-gauge or 19-gauge endoscopic ultrasound aspiration needle (Expect, Boston Scientific) and secured with a fixed length tube and probe latching mechanism to ensure that its distal end is completely inside the FNA needle. The subject was administered sedation and supplemental oxygen was used. The echoendoscope was introduced through the mouth and advanced to the duodenum (Fig. 3). After pancreatic EUS examination, the FNA needle was inserted into the echoendoscope, and the cyst was punctured under ultrasound guidance. The spatial gating probe was then extended 2 mm beyond the tip of the needle (Fig. 3a) with the probe latching mechanism and locked in that position with the locking button. By moving and angling the needle tip slightly, from 7 to 31 locations were measured (depending on the size of the cyst) covering a portion of the forward hemisphere of the internal cyst surface under EUS guidance (Fig. 3b, Supplementary Videos 1 and 2). The total LSS measurement time was less than 2 minutes. Then the spatial gating probe was removed, a 10 ml syringe was attached to the proximal end of the needle and the aspirated fluid was collected in the standard fashion. In 13 out of 14 procedures performed, the aspirated cyst fluid was found to be clear, however, in one case it appeared turbid on visual examination. In that case a separate 10 ml syringe with isotonic saline solution was used to replace the cyst contents[30], thereby expanding it back to the original size, and the data was retaken. After the procedure the aspirated fluid was sent for cytological and biochemical analysis.

The *in vivo* results are summarized in Table 2 and Figure 4. The only available gold standard for pancreatic cyst lesion *in vivo* malignancy diagnosis is either histopathology or survival with follow-ups, showing no indication of cancer development. Untreated cystic malignancy has a median survival of 3 months and a one-year survival rate of less than 10%[31]. Thus, a one-year follow-up after LSS measurement would identify the vast majority of previously undetected malignancies due to the rapid progression of this disease. Within our 14 *in vivo* patient set, two had definitive histopathology diagnoses, one was classified by our technology as cancer but misdiagnosed by cytology as negative for malignancy and the patient has died of metastatic cancer, one had definitive adenocarcinoma cytology diagnosis (though cytology has poor sensitivity it is very accurate when identifying cancer[32]) and five have survived for more than a year with follow-ups showing no evidence of malignancy. We consider the diagnosis of these 9 patients as reliable according to the above gold standard. Five remaining patients were only recently measured by our technique, and therefore do not have sufficient survival follow-up after the measurement. For those subjects, an independent assessment of the cysts by two expert gastroenterologists was obtained, who took into

account the clinical history (4 of the 5 cysts had a long history of cystic lesions with no malignancy progression), cytology results, CEA levels, and imaging results on interval growth, but were blinded to the LSS findings. If the resulting diagnosis was in agreement, the consensus assessment was used as a secondary endpoint.

The diagnostic parameter Δ for the malignant category is significantly higher than that for the non-malignant category ($P < 0.05$). All cysts with definitive diagnosis were identified correctly by LSS for the presence of malignancy (differential diagnosis between cancer, HGD, and cystic neuroendocrine tumor (CNET) lesions[33] was not evaluated, since the therapeutic choice would be the same). The accuracy for all 14 patients with both definitive diagnosis and consensus assessment is 93% (95% CI: 69%–99%).

Discussion

Pancreatic cysts are now being discovered in large numbers of patients due to the increased use of high resolution CT and MRI diagnostic imaging, with as many as 14% of MRI scans and 3% of CT scans incidentally discovering the presence of pancreatic cysts[34–36]. Because some pancreatic cysts are precancerous, and because pancreatic cancer is such a deadly condition, diagnosing the type of pancreatic cyst lesion accurately is a high stakes challenge. Despite the recent improvements in CT and MRI methodologies, these imaging approaches are unable to distinguish cancerous, premalignant and benign cysts reliably, in part due to a lack of sensitivity to cellular structure and biochemical properties, with wide variations in the reported accuracy ranging from 20% to 80%[37]. EUS is still the most sensitive technique currently available for the detection of small (<2–3 cm) pancreatic cysts[38,39], however, the accuracy of EUS for distinguishing mucinous from non-mucinous cysts is only 51%[6]. Because imaging techniques have a limited ability of identifying the type of pancreatic cyst, there has been a major effort to identify the cyst type with cyst fluid obtained during EUS-FNA procedures.

Cyst fluid can be analyzed for cytological findings, protein constituents, molecular markers, viscosity and DNA. The accuracy of cyst fluid analysis depends on the volume of cyst fluid obtained and therefore the size of the cyst. Recently, a large multicenter prospective clinical study evaluated both cytology and CEA for their ability to diagnose mucinous cystic lesions based on EUS-FNA in 341 patients. Pancreatic surgical resections of 112 of these patients found that cytology of cyst fluid has a sensitivity of 35% and a specificity of 83% for diagnosing mucinous vs. non-mucinous cysts and just 22% sensitivity for detecting mucinous cystic cancers[6]. Apart from CEA, the diagnostic potential of other molecular markers including amylase[40], cancer antigen (CA) 19-9[41,42], DNA[43], and fluid viscosity[44] have been investigated, with CEA being the only marker that achieves enough accuracy to be of clinical utility. However, CEA addition provides only a slight improvement over cytology alone in distinguishing between benign and mucinous cysts[6]. Due to the limited performance of existing cytological and molecular markers, a strong need is present to augment existing cyst fluid analysis approaches with an accurate diagnostic test.

Recently genetic mutations in genes such as guanine nucleotide binding protein, alpha stimulating (GNAS), and mutational profiles of targeted next-generation sequencing of

cancer genes, have been suggested as an adjunct to cytology and CEA to improve the diagnosis of mucinous cysts and to identify early malignancy within lesions by analyzing cyst fluid[45–47]. These studies are quite promising in substantiating the feasibility of detecting DNA mutations in IPMN using cyst fluid, even when these molecules are at low concentrations, though the performance of these genetic markers needs to be further evaluated in prospective *in vivo* clinical studies.

In our *in vivo* and *ex vivo* pilot studies native contrast LSS correctly identified the malignant potential of 21 out of 22 cystic lesions from 20 subjects in a double-blind comparison with either postoperative histopathology or survival outcomes achieving 95% accuracy (95% CI: 78%–99%) for identifying the presence of malignancy. This result is sufficiently powered to demonstrate a significant improvement over cytology (P=0.002), which has an accuracy of 58% (95% CI: 50%–65%)[7]. The resulting sensitivity is 90% (95% CI: 60–98%) and specificity is 100% (95% CI: 76–100%). In the *in vivo* studies the technique demonstrated the capability of obtaining data in part of the forward hemisphere of the internal cyst surface with a point probe and showed excellent agreement with the definitive diagnosis. To improve accuracy of the *in vivo* measurements, sampling of the larger fraction of the cyst wall could be beneficial.

We conclude that the LSS technique, which identifies malignant potential of pancreatic cystic lesions during regular EUS-FNA procedure, is rapid and inexpensive, offers great promise for distinguishing cancerous and precancerous cysts from benign cysts, and accurately identifies those pancreatic cysts that need surgical intervention. If this technique were to be used routinely, unnecessary pancreatoduodenectomies for benign lesions may be avoided and malignant cysts that otherwise could be missed may be identified.

Methods

Spatial gating probe

The spatial gating probe is designed to obtain a shallow single-scattering signal by collecting light at very small source-detector separations. Measurements at these sub-diffusion spatial separations have been shown to have a penetration depth of a few hundred micrometers[48]. The 0.45 mm outer diameter spatial gating probe (Fig. 2) consists of seven 100 μm core diameter fibers with a numerical aperture (NA) of 0.21 (Fig. 2c). A fiber in the outer ring of the probe is selected as the delivery fiber and is connected to a dedicated SMA connector, while three groups of collection fibers are selected to provide source-detector separations of 120, 220 and 240 μm and are terminated in three SMA connectors coupled to individual spectrometers. All of the fiber trunks are connected to a metal ferrule. The probe jacket is made of a robust medical grade biocompatible polyimide.

The spatial gating fiber optic probe inserted in the EUS-FNA needle is shown in Fig. 2a. To precisely control the 2 mm extension of the probe tip beyond the beveled needle tip (Fig. 2b), we designed and 3D printed the probe latching mechanism (Supplementary Video 3). The mechanism can be toggled to extend (Fig. 2e) or retract (Fig. 2f) the probe tip from the needle and locked in those positions with the locking button. One of the sides of the probe latching mechanism has a Luer lock connection for attaching it to the probe ferrule (Fig. 2d).

The other side is attached to the fixed length tube, which can be locked on the needle handle with a similar Luer lock (Fig. 2g). The probe is connected to the optical spectroscopy clinical system with the delivery fiber coupled to a 75W Xenon arc lamp source (Apex, Newport) at the proximal end and the collection fibers are coupled to fiber optic spectrometers (AvaSpec, Avantes).

Diagnostic algorithm

To obtain the diagnostic parameter Δ (Fig. 3c) collected with the spatial gating probe we utilize the fact that the contribution of backscattering to the total spatially resolved reflectance decreases with the increase in source-detector separation r, significantly faster than that of the multiple scattering signal[27]. Supplementary Figure 1 shows contribution of the single large angle backscattering component and the diffuse reflectance component in epithelial tissue with a reduced scattering coefficient[49] $\mu_s^{'}=3\,\mathrm{mm}^{-1}$ for the closest (r_1 = 120 μm) and farthest (r_2 = 240 μm) fibers in the spatial gating probe. From here it is clear that while total reflectance should be calculated as a sum of the diffuse reflectance and single large angle backscattering for the closest fiber, it can be accurately approximated with the diffuse reflectance from the farthest one alone.

In the 600 nm to 800 nm wavelength range tissue absorption can be ignored and the diffuse reflectance for the detector fiber i can be written as

$$R_i^d\left[\mu_s^{'}(\lambda)\right]=\frac{1}{\pi^2 r_s^2 r_i^2}\int_{A_s} dA_s \int_{A_i} dA_i R^d\left[\mu_s^{'}(\lambda)\,|\mathbf{r}_s-\mathbf{r}_i|\right] \quad (1)$$

where R^d is the well-known diffuse reflectance density[26,50]. The integrals here are numerically calculated over the area of the source fiber A_s with radius r_s and collection fibers A_i with radii r_i (i =1, 2).

Therefore, utilizing spectral measurements $S_1(\lambda)$ and $S_2(\lambda)$ by collection fibers 1 and 2, respectively, we get the following system of equations

$$\begin{aligned} R_1^d\left[\mu_s^{'}(\lambda)\right]+R^b(\lambda)&=S_1(\lambda)\\ R_2^d\left[\mu_s^{'}(\lambda)\right]&=S_2(\lambda)\end{aligned} \quad (2)$$

where $R^b(\lambda)$ is the single large angle backscattering component (Fig. 3d). This component carries diagnostic information and has been previously evaluated from the polarization gated data[13].

We used phantom experiments to isolate $R^b(\lambda)$ by removing the multiple scattering contribution in the system of equations (2). This contribution, in the case of weak absorption, has the same spectral dependence for both fibers. This can be understood by considering that multiple scattering is primarily $\mu_s^{'}(\lambda)$ dependent near the point of entry.

Therefore, using phantoms, we can calibrate the multiple scattering component in both fibers to make sure it can be cancelled. Phantoms with scattering coefficients close to that of tissue from 0.5 μm and 0.99 μm diameter polystyrene beads (Polysciences) in agarose gel (Sigma) were measured. These phantoms had the same $\mu_s'(\lambda)$ but different phase functions and produced a nearly identical calibration coefficient for balancing the multiple scattering component in the two fibers.

Human subjects

The feasibility of LSS in identifying precursor pancreatic cystic lesions and early stage pancreatic cancers was tested *ex vivo* in freshly resected pancreatic samples of eleven human subjects who underwent surgery for high risk pancreatic cysts and then *in vivo* during standard EUS-FNA procedures in another fourteen subjects who were undergoing initial EUS evaluation for pancreatic cysts. Both protocols were reviewed by the Institutional Review Board of Beth Israel Deaconess Medical Center and the requisite approvals were obtained.

In the *in vivo* study, consecutive patients undergoing EUS-FNA procedures for known pancreatic cystic lesions were enrolled. The inclusion criteria were as follows: (i) males and females older than 21 years old with pancreatic cyst(s); (ii) referred for EUS-FNA procedure; (iii) willing and able to provide written informed consent. We explained the procedure, indications, preparation, and potential complications to the subjects, who indicated their understanding and signed the corresponding consent forms.

We reviewed medical records of the patients within our study for the purpose of comparing the accuracy of the developed technique with the standard-of-care. The medical records, reviewed retrospectively after LSS diagnosis, included reports from MRI and CT imaging, cytology, histopathology, and cyst fluid biochemistry.

Statistical analyses

Significance between two groups of pancreatic cysts with and without malignant potential for *in vivo* and *ex vivo* data sets was determined by a two-tailed Wilcoxon rank sum test (IBM SPSS Statistics 23). Data were inferred as statistically significant if P values were <0.05. Confidence intervals were calculated according to the Wilson score method[51]. The chi-square test was used for comparing diagnostic accuracy with cytology. No statistical test was used to predetermine the sample size. The investigators were double blinded during the measurements and outcome assessment.

Code availability

The diagnostic algorithm is described in detail in the Methods section. We have opted not to make the data acquisition and processing code available because the code is proprietary and used for other projects.

Data availability

The data that support the findings of this study are available in figshare with the identifier doi:10.6084/m9.figshare.4496039 (ref. 52). The authors declare that all other data

supporting the findings of this study are available within the paper and its supplementary information.

Supplementary Material

Refer to Web version on PubMed Central for supplementary material.

Acknowledgments

We thank Yuping Li for help in data acquisition. This work was supported by US National Institutes of Health grants R01 EB003472 and R01 CA205431 and US National Science Foundation grants CBET-1402926 and CBET-1605116.

References

1. Collisson EA, et al. Subtypes of pancreatic ductal adenocarcinoma and their differing responses to therapy. Nat Med. 2011; 17:500–503. [PubMed: 21460848]
2. Brand RE, et al. Advances in counselling and surveillance patients at risk for pancreatic cancer. Gut. 2007; 56:1460–1469. [PubMed: 17872573]
3. Ryan DP, Hong TS, Bardeesy N. Pancreatic adenocarcinoma. N Engl J Med. 2014; 371:1039–1049. [PubMed: 25207767]
4. de Oliveira PB, Puchnick A, Szejnfeld J, Goldman SM. Prevalence of incidental pancreatic cysts on 3 Tesla magnetic resonance. PLoS ONE. 2015; 10:e0121317. [PubMed: 25798910]
5. Brugge WR, Lauwers GY, Sahani D, Fernandez-del Castillo C, Warshaw AL. Cystic neoplasms of the pancreas. N Engl J Med. 2004; 351:1218–1226. [PubMed: 15371579]
6. Brugge WR, et al. Diagnosis of pancreatic cystic neoplasms: a report of the cooperative pancreatic cyst study. Gastroenterology. 2004; 126:1330–1336. [PubMed: 15131794]
7. Cizginer S, et al. Cyst fluid carcinoembryonic antigen is an accurate diagnostic marker of pancreatic mucinous cysts. Pancreas. 2011; 40:1024–1028. [PubMed: 21775920]
8. Distler M, Aust D, Weitz J, Pilarsky C, Grützmann R. Precursor lesions for sporadic pancreatic cancer: PanIN, IPMN, and MCN. Biomed Res Int. 2014; 2014:474905. [PubMed: 24783207]
9. Singh M, Maitra A. Precursor lesions of pancreatic cancer: molecular pathology and clinical implications. Pancreatology. 2007; 7:9–19. [PubMed: 17449961]
10. Birkmeyer JD, et al. Hospital volume and surgical mortality in the United States. N Engl J Med. 2002; 346:1128–1137. [PubMed: 11948273]
11. Kosmahl M, et al. Cystic neoplasms of the pancreas and tumor-like lesions with cystic features: a review of 418 cases and a classification proposal. Virchows Arch. 2004; 445:168–178. [PubMed: 15185076]
12. Perelman LT, et al. Observation of periodic fine structure in reflectance from biological tissue: a new technique for measuring nuclear size distribution. Phys Rev Lett. 1998; 80:627–630.
13. Qiu L, et al. Multispectral scanning during endoscopy guides biopsy of dysplasia in Barrett's esophagus. Nat Med. 2010; 16:603–606. [PubMed: 20383155]
14. Sokolov K, Drezek R, Gossage K, Richards-Kortum R. Reflectance spectroscopy with polarized light: is it sensitive to cellular and nuclear morphology. Opt Express. 1999; 5:302–317. [PubMed: 19401735]
15. Yu CC, et al. Assessing epithelial cell nuclear morphology by using azimuthal light scattering spectroscopy. Opt Lett. 2006; 31:3119–3121. [PubMed: 17041654]
16. Terry NG, et al. Detection of dysplasia in Barrett's esophagus with *in vivo* depth-resolved nuclear morphology measurements. Gastroenterology. 2011; 140:42–50. [PubMed: 20854820]
17. Qiu L, et al. Spectral imaging with scattered light: from early cancer detection to cell biology. IEEE J Sel Top Quant Elect. 2012; 18:1073–1083.

18. Wax A, Chalut K. Nuclear morphology measurements with angle-resolved low coherence interferometry for application to cell biology and early cancer detection. Anal Cell Pathol. 2011; 34:207–222.
19. Wilson JD, Foster TH. Mie theory interpretations of light scattering from intact cells. Opt Lett. 2005; 30:2442–2444. [PubMed: 16196346]
20. Schuele G, et al. Optical spectroscopy noninvasively monitors response of organelles to cellular stress. J Biomed Opt. 2005; 10:051404. [PubMed: 16292941]
21. Itzkan I, et al. Confocal light absorption and scattering spectroscopic microscopy monitors organelles in live cells with no exogenous labels. Proc Natl Acad Sci USA. 2007; 104:17255–17260. [PubMed: 17956980]
22. Mourant JR, et al. Light scattering from cells: the contribution of the nucleus and the effects of proliferative status. J Biomed Opt. 2000; 5:131–137. [PubMed: 10938776]
23. Drezek R, et al. Light scattering from cervical cells throughout neoplastic progression: influence of nuclear morphology, DNA content, and chromatin texture. J Biomed Opt. 2003; 8:7–16. [PubMed: 12542374]
24. Hsiao A, Hunter M, Greiner C, Gupta S, Georgakoudi I. Noninvasive identification of subcellular organization and nuclear morphology features associated with leukemic cells using light-scattering spectroscopy. J Biomed Opt. 2011; 16:037007. [PubMed: 21456879]
25. van der Waaij LA, van Dullemen HM, Porte RJ. Cyst fluid analysis in the differential diagnosis of pancreatic cystic lesions: a pooled analysis. Gastrointest Endosc. 2005; 62:383–389. [PubMed: 16111956]
26. Farrell TJ, Patterson MS, Wilson B. A diffusion theory model of spatially resolved, steady-state diffuse reflectance for the noninvasive determination of tissue optical properties *in vivo*. Med Phys. 1992; 19:879–888. [PubMed: 1518476]
27. Vitkin E, et al. Photon diffusion near the point-of-entry in anisotropically scattering turbid media. Nat Commun. 2011; 2:587. [PubMed: 22158442]
28. Chandrasekhar, S. Radiative Transfer. Dover Publications, Inc; New York, NY: 1960.
29. Yoo KM, Liu F, Alfano RR. When does the diffusion approximation fail to describe photon transport in random media? Phys Rev Lett. 1990; 64:2647–2650. [PubMed: 10041774]
30. DeWitt J, McGreevy K, Schmidt CM, Brugge WR. EUS-guided ethanol versus saline solution lavage for pancreatic cysts: a randomized, double-blind study. Gastrointest Endosc. 2009; 70:710–723. [PubMed: 19577745]
31. Simons JP, et al. Malignant intraductal papillary mucinous neoplasm: are we doing the right thing? J Surg Res. 2011; 167:251–257. [PubMed: 19765732]
32. Oguz D, et al. Accuracy of endoscopic ultrasound-guided fine needle aspiration cytology on the differentiation of malignant and benign pancreatic cystic lesions: a single-center experience. J Dig Dis. 2013; 14:132–139. [PubMed: 23167591]
33. Baker MS, et al. Pancreatic cystic neuroendocrine tumors: preoperative diagnosis with endoscopic ultrasound and fine-needle immunocytology. J Gastrointest Surg. 2008; 12:450–456. [PubMed: 18157720]
34. Winter JM, et al. Periampullary and pancreatic incidentaloma: a single institution's experience with an increasingly common diagnosis. Ann Surg. 2006; 243:673–683. [PubMed: 16633003]
35. Lee KS, Sekhar A, Rofsky NM, Pedrosa I. Prevalence of incidental pancreatic cysts in the adult population on MR imaging. Am J Gastroenterol. 2010; 105:2079–2084. [PubMed: 20354507]
36. Laffan TA, et al. Prevalence of unsuspected pancreatic cysts on MDCT. AJR Am J Roentgenol. 2008; 191:802–807. [PubMed: 18716113]
37. Boot C. A review of pancreatic cyst fluid analysis in the differential diagnosis of pancreatic cyst lesions. Ann Clin Biochem. 2014; 51:151–166. [PubMed: 24097809]
38. Yasuda K, Mukai H, Nakajima M. Endoscopic ultrasonography diagnosis of pancreatic cancer. Gastrointest Endosc Clin N Am. 1995; 5:699–712. [PubMed: 8535618]
39. DeWitt J, et al. Comparison of endoscopic ultrasonography and multidetector computed tomography for detecting and staging pancreatic cancer. Ann Intern Med. 2004; 141:753–763. [PubMed: 15545675]

40. Park WG, et al. Diagnostic performance of cyst fluid carcinoembryonic antigen and amylase in histologically confirmed pancreatic cysts. Pancreas. 2011; 40:42–45. [PubMed: 20966811]
41. Steinberg W. The clinical utility of the CA 19-9 tumor-associated antigen. Am J Gastroenterol. 1990; 85:350–355. [PubMed: 2183589]
42. Kim JE, et al. Clinical usefulness of carbohydrate antigen 19-9 as a screening test for pancreatic cancer in an asymptomatic population. J Gastroenterol Hepatol. 2004; 19:182–186. [PubMed: 14731128]
43. Khalid A, et al. Pancreatic cyst fluid DNA analysis in evaluating pancreatic cysts: a report of the PANDA study. Gastrointest Endosc. 2009; 69:1095–1102. [PubMed: 19152896]
44. Bick BL, et al. The string sign for diagnosis of mucinous pancreatic cysts. Endoscopy. 2015; 47:626–631. [PubMed: 25730281]
45. Wu J, et al. Recurrent GNAS mutations define an unexpected pathway for pancreatic cyst development. Sci Transl Med. 2011; 3:92ra66.
46. Amato E, et al. Targeted next generation sequencing of cancer genes dissects the molecular profiles of intraductal papillary neoplasms of the pancreas. J Pathol. 2014; 233:217–227. [PubMed: 24604757]
47. Wu J, et al. Whole-exome sequencing of neoplastic cysts of the pancreas reveals recurrent mutations in components of ubiquitin-dependent pathways. Proc Natl Acad Sci USA. 2011; 108:21188–21193. [PubMed: 22158988]
48. Amelink A, Bard MP, Burgers SA, Sterenborg HJ. Single-scattering spectroscopy for the endoscopic analysis of particle size in superficial layers of turbid media. Appl Opt. 2003; 42:4095–4101. [PubMed: 12868852]
49. Mutyal NN, et al. *In vivo* risk analysis of pancreatic cancer through optical characterization of duodenal mucosa. Pancreas. 2015; 44:735–741. [PubMed: 25906443]
50. Zonios G, et al. Diffuse reflectance spectroscopy of human adenomatous colon polyps *in vivo*. Appl Opt. 1999; 38:6628–6637. [PubMed: 18324198]
51. Newcombe RG. Two-sided confidence intervals for the single proportion: comparison of seven methods. Stat Med. 1998; 17:857–872. [PubMed: 9595616]
52. Zhang, L., et al. Dataset for light scattering spectroscopy identifies the malignant potential of pancreatic cysts during endoscopy. figshare. 2016. http://dx.doi.org/10.6084/m9.figshare.4496039

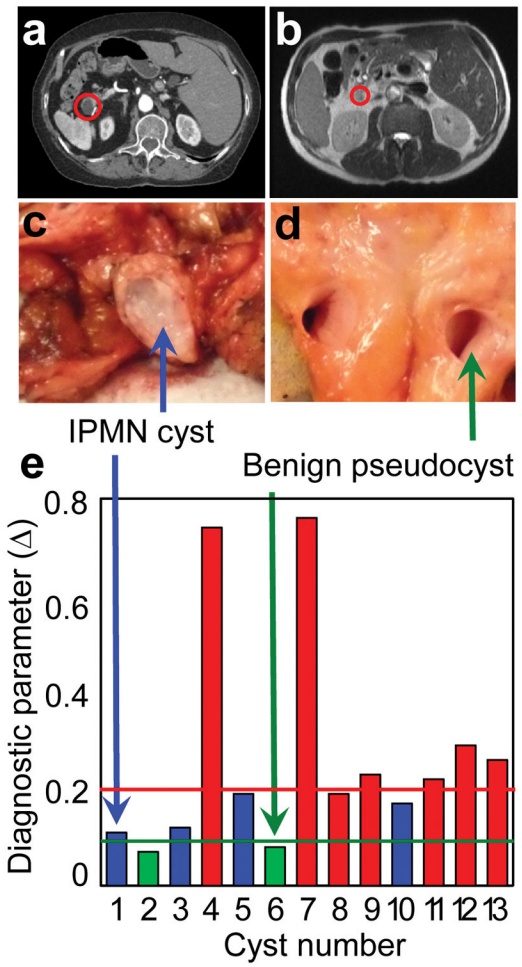

Figure 1. ***Ex vivo*** **optical spectroscopic differentiation of cystic neoplasms**

(a) Abdominal and pelvic CT angiography in subject 1. **(b)** Magnetic resonance cholangiopancreatography (MRCP) in subject 6. **(c, d)** Cross sectional cut photographs of corresponding pancreatic resection samples with cysts clearly seen. **(e)** Diagnostic parameter Δ for 13 cyst measurements with red bars indicating cysts diagnosed by histopathology as HGD, blue as LGD IPMN and green as benign, with green and red lines representing diagnostic algorithm LGD and HGD/Cancer cut-offs, respectively. Cysts 1 and 2 are from the first subject, and cysts 10 and 11 are from the ninth subject.

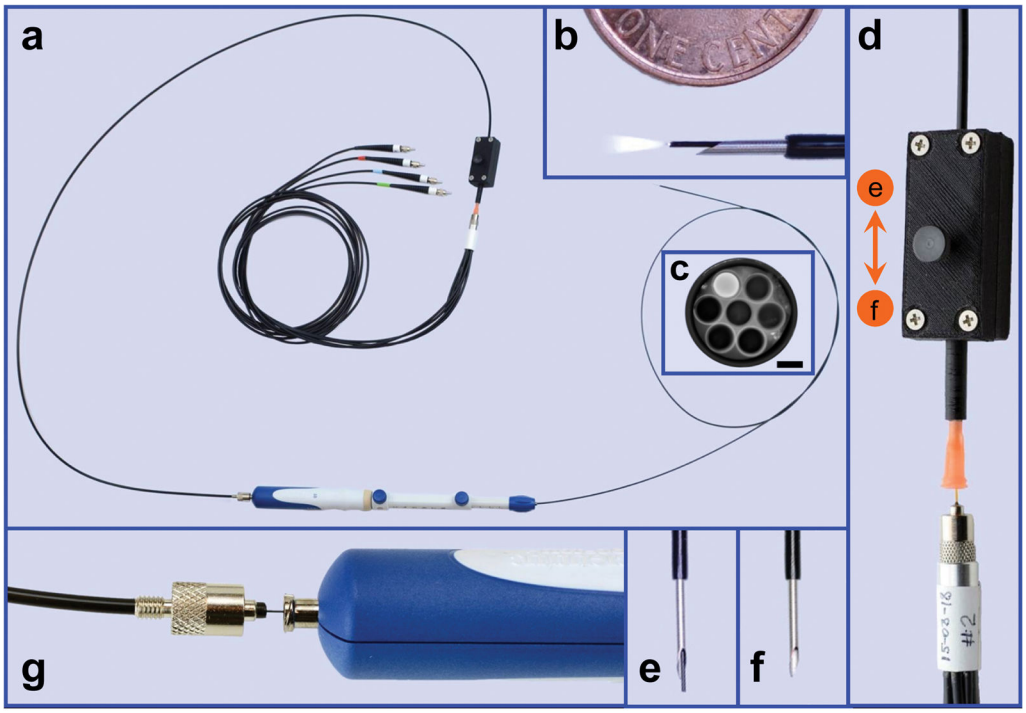

Figure 2. ***In vivo*** **spatial gating fiber optic probe for use with EUS-FNA**

(a) The probe inserted in the FNA needle. Three SMA connectors at the proximal end for coupling groups of fibers with 120 μm, 220 μm and 240 μm distal end source-detector separations with three individual spectrometers and another SMA connector for coupling delivery fiber with the broadband light source. **(b)** Probe extended by 2 mm from the beveled needle tip with the source on and a US penny for scale. **(c)** Distal tip of the probe. The 450 μm outer diameter probe consists of seven 100 μm core diameter fibers with NA=0.21. The probe jacket is made of a robust medical grade biocompatible polyimide. The delivery fiber in the outer ring is illuminated. Scale bar - 100 μm. **(d)** Probe latching mechanism and fixed length tube. The mechanisms can be locked with the position locking button **(d)** and toggled to extend **(e)** or retract **(f)** the probe tip from the needle. **(g)** Fixed length tube locked on the needle handle with Luer lock connection.

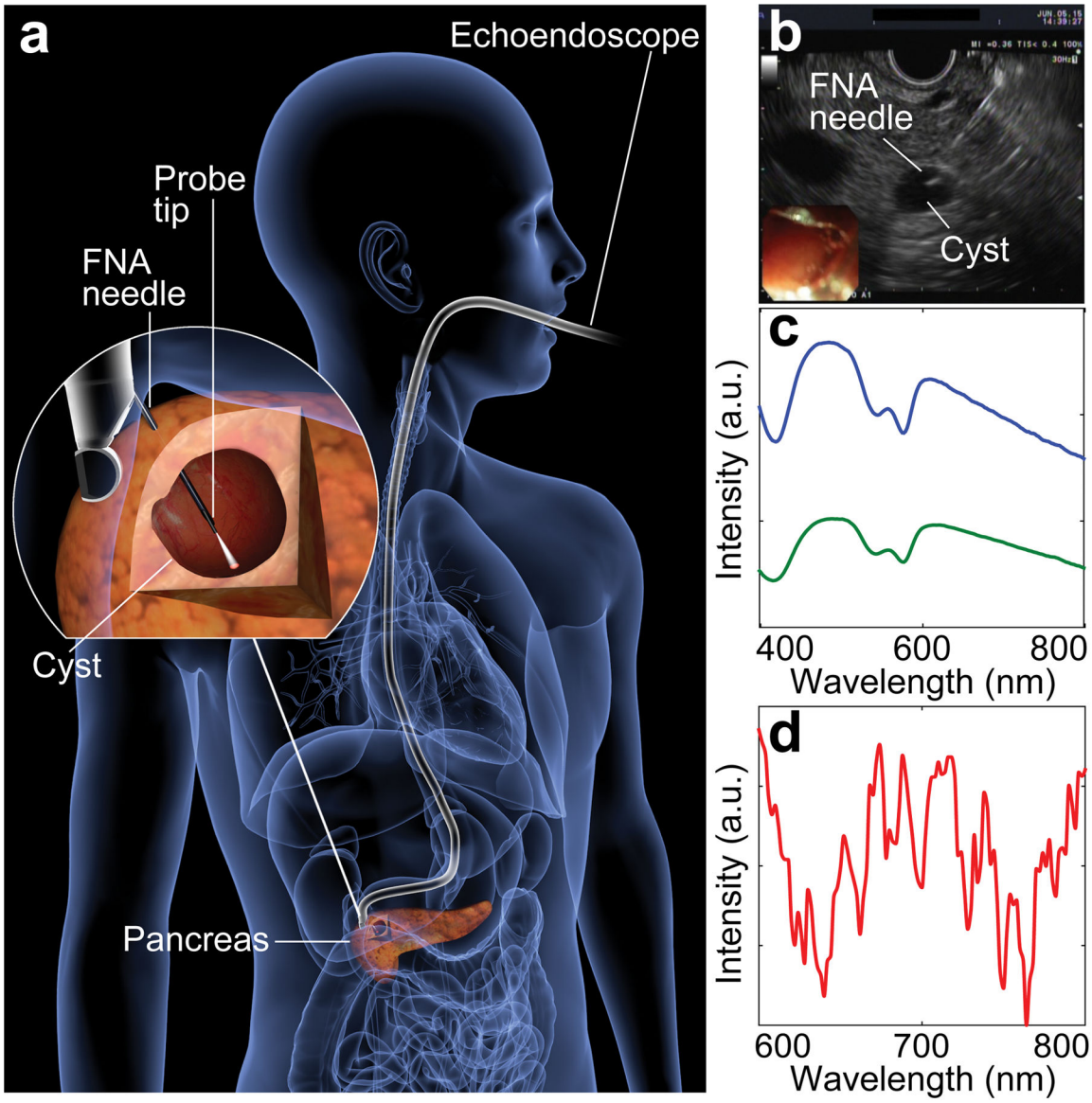

Figure 3. ***In vivo*** **measurements during endoscopic ultrasound-guided fine-needle aspiration (EUS-FNA) procedure**

(a) Illustration depicting spatially gated LSS measurements of the internal cyst surface. Introduced through the mouth echoendoscope is advanced to the duodenum and the cyst is punctured under the ultrasound guidance with the FNA needle. The probe tip is extended from the needle, illuminating a location of the internal cyst surface. The inset shows details of the measurements. **(b)** EUS image of the FNA needle penetrating the cyst with the LSS probe inserted. **(c)** Typical spectra collected in the cyst at 120 μm (blue line) and 240 μm (green line) source-detector separations. **(d)** The backscattering component obtained from the spectra at both 120 μm and 240 μm source-detector separations presented in (c).

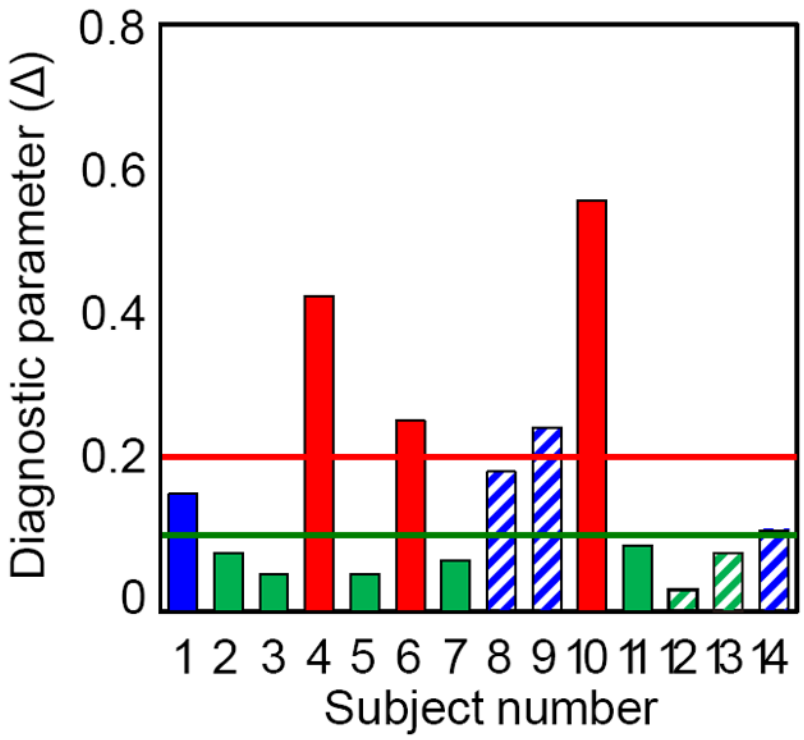

Figure 4. ***In vivo*** **optical spectroscopic differentiation of cystic neoplasms in 14 subjects**

Diagnostic parameter vs. diagnostic gold standard and secondary endpoint. The solid bars represent the diagnostic gold standard, obtained from postoperative/postmortem histopathology or survival with follow-ups. The solid red color represents adenocarcinoma or CNET, solid blue represents LGD IPMN, and solid green represents benign. Following the same color scheme, the striped bars represent the diagnostic secondary endpoint of an independent consensus assessment of the cysts by two expert gastroenterologists. Green and red lines represent LGD and HGD/Cancer diagnostic algorithm cut-offs, respectively.

Table 1

***Ex vivo* differentiation of cystic neoplasms**

Polarization gated LSS optical spectroscopic technique *vs.* MRI/CT, CEA level, preoperative cytology, and postoperative histopathology. The two last columns present Δ parameter and the LSS diagnosis. MRI includes both abdominal MRI and MRCP. CNET - cystic neuroendocrine tumor; ITPN - intraductal tubulopapillary neoplasm. Empty cells represent no information due to lack of imaging classification, cellular material or absence of data on CEA level.

Cyst	MRI/CT	CEA (ng/ml)	Cytology	Histopathology cyst type	Histopathology diagnosis	LSS (Δ)	LSS diagnosis
1[a]	CNET	686	-	IPMN	LGD	0.11	LGD
2[a]	-	-	-	Serous	Benign	0.07	Benign
3	Serous	67	Scant benign cells	IPMN	LGD	0.12	LGD
4	IPMN	142	-	IPMN	HGD	0.74	HGD
5	IPMN	430	LGD IPMN	IPMN	LGD	0.19	LGD
6	-	-	-	Pseudocyst	Benign	0.08	Benign
7	-	-	HGD IPMN	IPMN	HGD	0.76	HGD
8	IPMN	1.8	HGD IPMN	IPMN	HGD	0.19	LGD
9	IPMN	151	HGD	IPMN	HGD	0.23	HGD
10[b]	IPMN	-	-	IPMN	LGD	0.17	LGD
11[b]	IPMN	-	Adenocarcinoma	IPMN	HGD	0.22	HGD
12	IPMN	-	Carcinoma	ITPN	HGD	0.29	HGD
13	IPMN	122	HGD IPMN	IPMN	HGD	0.26	HGD

[a] cysts 1 and 2 are from the same subject

[b] cysts 10 and 11 are from the same subject

Table 2

***In vivo* differentiation of cystic neoplasms in 14 subjects**

Spatially gated LSS optical spectroscopic technique *vs.* MRI/CT, CEA level, cyst size, cytology, and the resulting diagnosis. The source of the resulting diagnosis is either histopathology, gastroenterologists' consensus assessment (GCA), or conclusive diagnosis (CD), combining more than one-year follow-up with GCA. Two last columns present Δ parameter and LSS diagnosis. MRI includes both abdominal MRI and MRCP. ACC - acinar cell carcinoma; CNET - cystic neuroendocrine tumor. Empty cells represent no information due to lack of imaging classification or absence of data on CEA level.

Subject	MRI/CT	CEA (ng/ml)	Size (mm)	Cytology	Source of diagnosis	Diagnosis	LSS (Δ)	LSS diagnosis
1	IPMN	7.8	11	LGD IPMN	CD	LGD IPMN	0.16	LGD
2	MCN	21	49	Degenerated glandular debris	CD	Benign	0.08	Benign
3	Serous	370	27	Acellular specimen	CD	Benign	0.05	Benign
4	Pseudocyst	7.3	51	ACC or CNET	Histopathology	CNET	0.43	HGD/Cancer
5	IPMN	212	20	Benign paucicellular sample	CD	Benign	0.05	Benign
6	IPMN	3676	22	LGD IPMN	Died (cancer)	Cancer	0.26	HGD/Cancer
7	Serous	226	32	Negative for malignant cells	CD	Benign	0.07	Benign
8	IPMN	<1	37	Insufficient cellular material	GCA	IPMN	0.19	LGD
9	IPMN	9	20	Virtually acellular specimen	GCA	IPMN	0.25	HGD/Cancer
10	-	7290	57	Adenocarcinoma	Cytology[a]	Cancer	0.56	HGD/Cancer
11	IPMN	-	50	Negative for malignant cells	Histopathology	Pseudocyst	0.09	Benign
12	-	<1	29	Serous cystadenoma	GCA	Benign	0.03	Benign
13	Serous	-	28	Insufficient material	GCA	Benign	0.08	Benign
14	IPMN	2364	21	IPMN	GCA	LGD IPMN	0.11	LGD

[a] positive predictive value (PPV) of cytology when identifying cancer is 100%[32]